iCharacteristics of Trans-Critical Propane Spray Discharged from Multi-Hole GDI Injector

Zhang, Zhou; Li, Yanfei; Ma, Xiao; Ding, Haichun; Xu, Hongming; Wang, Zhi; Shuai, Shijin

DOI:
10.1016/j.expthermflusci.2018.07.025

Document Version
Peer reviewed version

Citation for published version (Harvard):
Zhang, Z, Li, Y, Ma, X, Ding, H, Xu, H, Wang, Z & Shuai, S 2018, 'iCharacteristics of Trans-Critical Propane Spray Discharged from Multi-Hole GDI Injector', *Experimental Thermal and Fluid Science*.
https://doi.org/10.1016/j.expthermflusci.2018.07.025

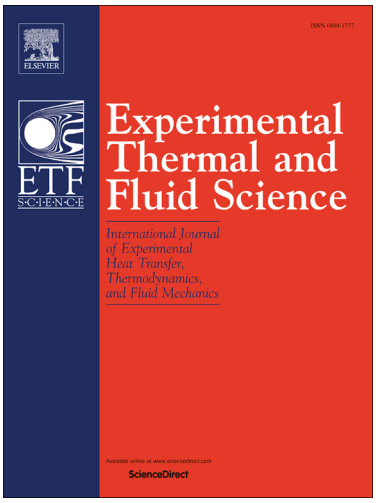

iCharacteristics of Trans-Critical Propane Spray Discharged from Multi-Hole GDI Injector

Zhou Zhang, Yanfei Li, Xiao Ma, Haichun Ding, Hongming Xu, Zhi Wang, Shijin Shuai

PII: S0894-1777(18)30166-3
DOI: https://doi.org/10.1016/j.expthermflusci.2018.07.025
Reference: ETF 9552

To appear in: *Experimental Thermal and Fluid Science*

Received Date: 7 February 2018
Revised Date: 21 May 2018
Accepted Date: 20 July 2018

Please cite this article as: Z. Zhang, Y. Li, X. Ma, H. Ding, H. Xu, Z. Wang, S. Shuai, iCharacteristics of Trans-Critical Propane Spray Discharged from Multi-Hole GDI Injector, *Experimental Thermal and Fluid Science* (2018), doi: https://doi.org/10.1016/j.expthermflusci.2018.07.025

Characteristics of Trans-Critical Propane Spray Discharged from Multi-Hole GDI Injector

Zhou Zhang[a], Yanfei Li[a], Xiao Ma[a,*], Haichun Ding[a], Hongming Xu[a,b], Zhi Wang[a], Shijin Shuai[a]

a. State Key Laboratory of Automotive Safety and Energy, Tsinghua University, Beijing 100084, China
b. University of Birmingham, Birmingham, B15 2TT, UK

* Corresponding Author, Phone: +86 13811176872, Email: max@tsinghua.edu.cn

Highlights

- Trans-critical and flash-boiling sprays of propane show the similarity in spray morphology.
- Shock structures near the nozzle are observed in trans-critical sprays of propane.
- Decreasing the injection pressure of trans-critical spray can induce a gas-like jet.
- Interaction of spray plumes increases Mach disk distance of trans-critical propane spray.

Abstract

This paper is to investigate the characteristics of trans-critical propane spray compared with the flash boiling spray ejected from a multi-hole injector in a constant volume chamber by using the Schlieren and backlit imaging methods. The fuel temperature (T_f) is set from 30 °C to 120 °C, injection pressure (p_f) from 60 bar to 120 bar and ambient pressure (p_a) from 0.2 bar to 10 bar.

The results show that the trans-critical spray has longer vapor penetration and shorter liquid penetration than the flash boiling spray, but those two sprays have similar curve liquid boundaries near the nozzle. Several discernable collapsed shock structures near the nozzle are observed at T_f=120 °C, p_f=120 bar, p_a=1 bar, but they disappear when p_f drops to 60 bar for the transition path may not enter the two-phase region, and the liquid phase hardly occurs. The Mach disk distance of trans-critical spray in this study is larger than that of the under-expanded ideal gas jet because of the collapse phenomenon. At T_f=120 °C, p_f=120 bar, the liquid length decreases when $p_a$increases from 0.2 bar to 2.5 bar and increases when p_a continues to rise.

Keywords: Propane; Trans-critical spray; GDI; Thermodynamic path.

Nomenclature

p_f	Injection pressure	$\bar{p}_r$	Reduced injection pressure
T_f	Fuel temperature	$\bar{T}_r$	Reduced fuel temperature
p_c	Critical pressure	s_f	Specific entropy of fuel
T_c	Critical temperature	h_f	Specific enthalpy of fuel
p_a	Ambient pressure	$p_{f,e}$	Nozzle exit pressure
$h_{f,e}$	Specific enthalpy at the nozzle exit	$a_{f,e}$	Speed of sound at the nozzle exit
$u_{f,e}$	Fluid speed at the nozzle exit	$Ma_{f,e}$	Mach number at the nozzle exit
L_1	Liquid penetration	X_i	distance of Mach disk

1. Introduction

The fossil fuel is still the primary power source of the vehicles. However, the massive consumption of fossil fuel by vehicles contributes to air pollution [1] and global warming [2]. Particle matter (PM) and CO_2 are strictly limited by new emission standards and regulations. Low-carbon alternative fuels have the promising to reduce the exhaust emissions from motor vehicles. LPG comprises short-chain alkanes, e.g., propane and butane, and therefore LPG combustion produces lower CO and HC emissions [3] and helps with a CO_2 reduction in comparison with gasoline [4]. Furthermore, the higher research octane number (RON) of LPG [5][6] allows a high compression ratio to improve fuel economy and to reduce CO_2.

The gasoline direct injection (GDI) technique has advantages in achieving higher power, better fuel economy and overall emissions [7], favored by modern vehicles. Over the past years, GDI engines have occupied the majority of the market share of engines for passenger cars and hybrid vehicles [8]. However, compared with the conventional port fuel injection (PFI) engine, GDI engines generate more particles [9][10]. Previous studies have demonstrated that the combination of direct injection (DI) and LPG can efficiently resolve the PM emission problems of spark ignition engines [11][12][13][14]. The spray characteristics, which substantially determine the combustion process and thus the engine performance and emissions of a DI engine, are worthy of study. Flash boiling will happen in LPG spray under most engine operating conditions[15]. Propane, as the main component of LPG, has similar spray characteristics to LPG. A thorough understanding of the micro and macro characteristics of propane spray will contribute to the research of LPG spray in DI engines. Lacey et al. [16] experimented on the spray characteristics of propane under engine operating conditions using Mie scattering and the Schlieren method and concluded that the thermodynamic property should be taken into consideration for propane sprays.

The critical temperature and pressure of propane are 96.74 °C (369.89K) and 42.5 bar[17], It is easy to make the trans-critical sprays possible, which may promote the mixing process and decrease exhaust emissions. According to Ref. [18], there are two types of trans-critical sprays: where a supercritical fluid is injected into subcritical surroundings and the fuel can be liquid or gas, or a high pressurized liquid with subcritical temperature is injected into an environment where the pressure is subcritical, but the temperature is supercritical. The first type may arise in propane sprays under engine conditions, which is the focus of this paper. Hereafter, the 'trans-critical spray' refers to the supercritical-to-subcritical fluid.

The studies on trans-critical sprays have attracted much attention in the aviation field. Wu et al. [19] investigated the characteristics of the trans-critical injection of ethylene with a customized single-hole injector using Schlieren. The experiment results showed that the flow was choked at the nozzle exit and there was a shock structure nearby; the trans-critical jet was similar to the under-expanded ideal gas jet when the fuel temperature was much higher than the critical temperature. The same research group then experimented with the expansion process of under-expanded supercritical ethylene jets into the superheated environment [20]. It was observed that higher ambient temperature reduced the length of the fuel condensation core, but it could not eliminate the core because of the limited heat transfer rate from the ambient gas to the spray plume. Star et al. [21] conducted a simulation on the same spray conditions, giving a well-matched simulation result. They found out that the masking effects of fuel condensation covered the Mach disk structure and the amounts of condensate increased with the increase of chamber pressure. Lin et al. [22][23] presented a database of the trans-critical injection of a methane/ethylene mixture into subcritical nitrogen and analyzed the structure and phase transition of this kind of injection. As for the research of automobile engines, the application of trans-critical spray did not appeal to researchers until recently when much higher injection pressure was applied to reduce the emissions in direct injection engines. Boer et al. [24] applied trans-critical gasoline injections in a GDI engine, and as a result, the emissions including PN, PM, BSHC, and CO dramatically decreased due to the increased mixture homogeneity. Zhang et al. [25] investigated the trans-critical spray characteristics of a multi-hole GDI injector by using high-speed imaging. They found that the trans-critical spray plumes collapsed and merged into one bigger jet, similar to the multi-jet flash boiling sprays[26]; when the initial fuel temperature was high enough, there was a Mach disk structure near the nozzle. There is an increasing interest in

understanding the characteristics of the trans-critical sprays which have the potential to decrease the PM emission, and more detailed investigations are required to have a better understanding of the trans-critical spray discharged from multi-hole GDI injection.

This paper aims to investigate the difference between the trans-critical spray and the flash boiling spray of propane and the influence of fuel condition and ambient pressure on the macroscopic characteristics of the trans-critical sprays of propane. The main parameters, including liquid penetration, vapor penetration, liquid length and Mach disk distance, were obtained by using speed backlit and Schlieren imaging methods. A *p-s* diagram was used to account for the injection process. The visible shock structures appeared, and the normalized Mach disk distance of the trans-critical spray was discussed to compare the trans-critical spray with the under-expanded ideal gas jet.

2. Experiment apparatus and conditions

2.1 Experimental set-up

The systems for high-speed backlit and Schlieren imaging are shown in Figure 1(a) and Figure 1(b), respectively. In Figure 1(a), the LED lamp (150W) and the high-speed camera (PhotronSA-X2) were placed on the opposite sides of the constant pressure. The full liquid spray can be captured by using this set-up with a Nikon 105mm lens, while the spray near the nozzle tip was captured by a Nikon 180mm lens. In the Schlieren system, a DC halogen tungsten lamp (24 V, 300 W) was used as the light source. Those two types of experiment were conducted separately. Both the high-speed backlit and Schlieren imaging used the same high-speed camera, and the camera speed was set at 40000 fps with a resolution of 512×584 pixels. The exposure time was 1/100000 second for the backlit imaging and 1/416999 second for the Schlieren imaging.

The propane was pressurized by high-pressure air in a storage tank. A fuel accumulator surrounded by several heaters was connected to the storage tank as the fuel rail, which can heat up the fuel to the target temperature and stabilize the injection pressure. The temperature of the fuel in the accumulator was regarded as the fuel temperature, it was measured by a thermocouple and controlled by a temperature controller. The other side of the fuel accumulator was connected to a

five-hole GDI injector with a diameter of 0.18 mm holes. The holes are distributed asymmetrically and form a slightly tilted spray when the sprays become collapsed. More details about this injector can be found in Ref.[27]. The injector was also heated by a heater-embedded adapter to maintain the temperature of the propane inside the injector during the consecutive injections. To minimize the effect of the air solubility in liquid propane, the accumulator was first heated up to the given value, and then the storage tank was pressurized by the high-pressure air. The propane was depressurized immediately after finishing each operating condition.

The constant pressure vessel was pressurized by the high-pressure air. A centrifugal pump was employed for scavenging and to create sub-atmospheric pressure conditions in the constant volume chamber when a sub-atmospheric pressure was needed. A house-made ECU was used to synchronize the injection and imaging timings for both the high-speed backlit and Schlieren imaging. The tests were repeated ten times for each operating condition to diminish the uncertainty of the results caused by the shot-to-shot variation. The injection duration was set to 1500 μs because 1500 μs was long enough for all the spray to form a steady form. The camera captured 100 pictures with a time interval of 25 μs. The scavenging was done for each test after the injection to guarantee the same ambience.

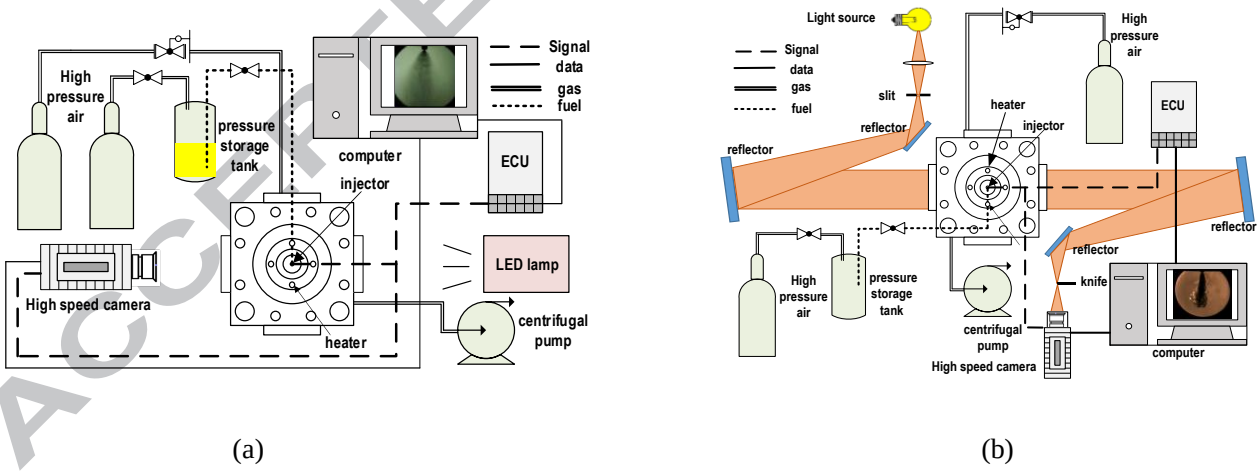

(a) (b)

Figure 1. Schematic of (a) high-speed imaging and (b) Schlieren detection system of trans-critical propane spray

2.2 Test conditions

Propane with a purity higher than 99.9% was used in this experiment. To investigate the trans-critical spray of propane, the injection pressure and fuel temperature must higher than the critical point. The flash boiling spray should also be included to give a comparison. Four fuel temperatures 30 °C, 80 °C, 100 °C, 120°C were selected to compare the

flash-boiling spray with trans-critical spray, and the injection pressure and the ambient pressure remained at 120 bar and 1bar, respectively. As for the detailed investigation of trans-critical spray, two fuel temperatures 100 °C, 120°C were selected, and the injection pressure was set from 60 bar to 120 bar. To investigate the effect of ambient pressure on trans-critical spray, the ambient pressure varied from 0.2 bar to 10 bar, and other parameters were fixed. The experimental operating conditions are listed in Table 1. The physical properties of propane at different experiment conditions are listed in the Appendix (A1). Two dimensionless numbers, $\bar{p}_r$ and $\bar{T}_r$ are introduced to reveal the state of propane under different operating conditions; where $\bar{p}_r = p_f/p_c$, $\bar{T}_r = T_f/T_c$, p_f and T_f are fuel pressure and temperature, p_c and T_c are the critical parameters of propane.

The operating conditions are also presented on the phase map of propane, as shown in Figure 2. The dots in Figure 2 represent the injection conditions, namely the initial thermal states of the fuel. The squares indicate the ambient conditions. The dashed-dotted arrow line refers to the phase change path of the flash boiling sprays, and the two solid arrow lines represent the path of the trans-critical sprays. According to the Ref. [28], flash boiling can occur by heterogeneous nucleation or homogeneous nucleation. As for the flash boiling sprays in this paper, the pressure drop rate is higher than the Hutcherson et al.[29,30] criterion, and the degree of superheat p_a/p_{sat} is much less than 0.3. Thus, it is assumed that the homogeneous nucleation dominates the nucleation process.

Table 1 Test operating conditions for high-speed backlit and Schlieren imaging

Objectives of the experiment	Injection pressure p_f /bar ($\bar{p}_r$)	Fuel temperature T_f /°C ($\bar{T}_r$)	Ambient pressure p_a /bar	Ambient temperature T_a /°C
Comparison of trans-critical spray and flash-boiling spray	120 (2.82)	30 (0.82), 80 (0.96), 100 (1.01), 120 (1.06)	1	20
Analysis of the characteristics of trans-critical spray	60 (1.41), 90 (2.11), 120 (2.82)	100 (1.01), 120 (1.06)	1	20
Effect of ambient pressure	120 (2.82)	120 (1.06)	0.2, 0.5, 0.8, 1, 2.5, 5, 10	20

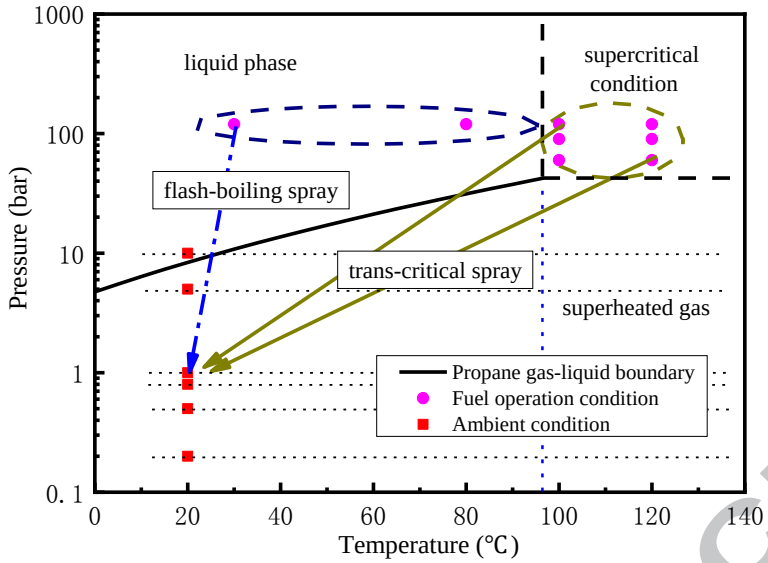

Figure 2. Experiment conditions

2.3 Image processing

There are five plumes when subcooled gasoline is used[27]. In this study, the spray plumes eventually merge into a dense one, namely collapse, for both flash boiling and trans-critical spray under most conditions. The merged spray plume can be regarded as one plume when calculating the penetrations and spray areas.

The processing of backlit pictures is shown in Figure 3. The background is subtracted by subtracting the spray images from the background images, and the white zone represents the liquid phase, as shown in figure 3a. Then the threshold is calculated by using Otsu's method [31] for each picture. The image was assumed to contain two classes of pixels following bi-modal histogram (liquid phase and background), the threshold was calculated by maximizing their intra-class variance. In Figure 3b, the liquid spray is extracted by using the threshold. In Figure 3c, the boundary of the liquid phase is detected by using the "edge" function of MATLAB based on the Sobel operator[32]. The liquid penetration is the distance between the far end of the boundary and the nozzle tip. The area surrounded by the boundary the backlit imaging picture is defined as "area of dense liquid phase". Figure 3d presents a good extraction result.

The extraction of the gas phase was more difficult than the liquid phase. Figure 4 presents the image process of the Schlieren picture. Figure 4a is the original picture. The background is subtracted, and then the absolute values of the subtracted picture are obtained, which is shown in Figure 4b. In Figure 4c, the grey values of the picture are normalized. An

average filter is used to reduce the noise of Figure 4c, shown in Figure 4d. In Figure 4e, the gas phase is extracted by using Otsu's method[31]. However, there are some separated areas and holes. The image closing operation is used to connect the whole gas phase, shown in Figure 4f. In Figure 4g, the boundary of the gas phase is detected by the Sobel operator[32]. The vapor penetration is the distance between the far end of the gas boundary and the nozzle tip. The area surrounded by the boundary in the Schlieren images is named "whole vapor area". Figure 4g shows that the extracted boundary overlaps on the original picture, giving a good matching result.

In Figure 5a-b, the shock structures that generate in highly under-expanded jet due to choking and expansion of spray are distinguished from the backlit imaging pictures. Figure 5c is the corresponding Schlieren image, and the merged shock structure can be distinguished. The area where there is a sudden increase in density of liquid phase due to a sudden change in pressure is the boundary of the shock structures, shown as the red dotted line. These shock structures also collapse towards the spray's center, and it is hard to separate the individual plumes. The red dotted line can be called envelope curve. The Mach disk of each jet cannot be identified due to the distortion and merging effect of the shock structures. However, the position where the orange dotted line locates is the farthest position of the merge shock structure, and this position has the same property as the position of Mach disk [20]. To avoid misunderstanding, we call this position "merged Mach disk area". The distance of Mach disk X_i in this paper is defined as the distance between the nozzle and the merged Mach disk area. As the result from the backlit image is more clear than Schlieren images due to its larger image resolution, the current study discusses X_i based on the backlit images. According to the calculation results, the extracted boundary of the dense liquid phase is bigger than the total size of the shock structures and the liquid penetration L_1 is larger than X_i. The area between the shock structures and the boundary of the liquid phase can be called "tail region" in which the liquid droplets may originate from the direct transition of supercritical fluid or the condensation of supersaturated vapor.

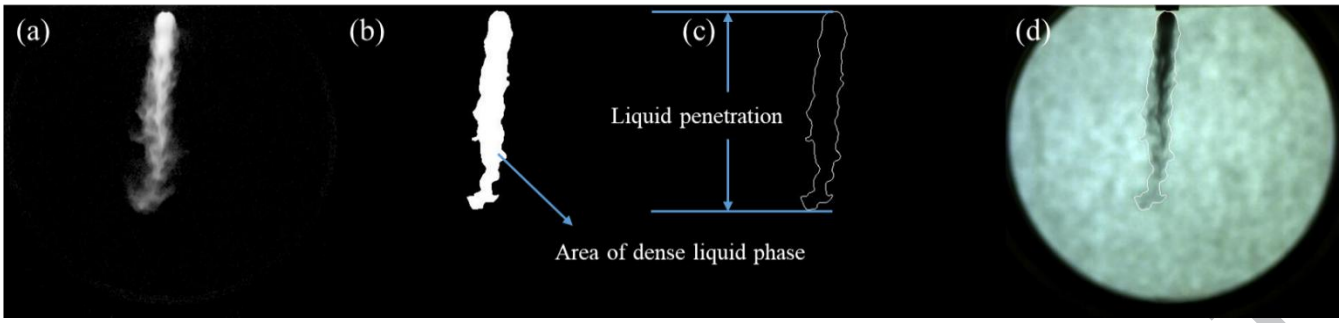

Figure 3. Image processing of backlit picture and the definitions of liquid penetration and area of dense liquid phase

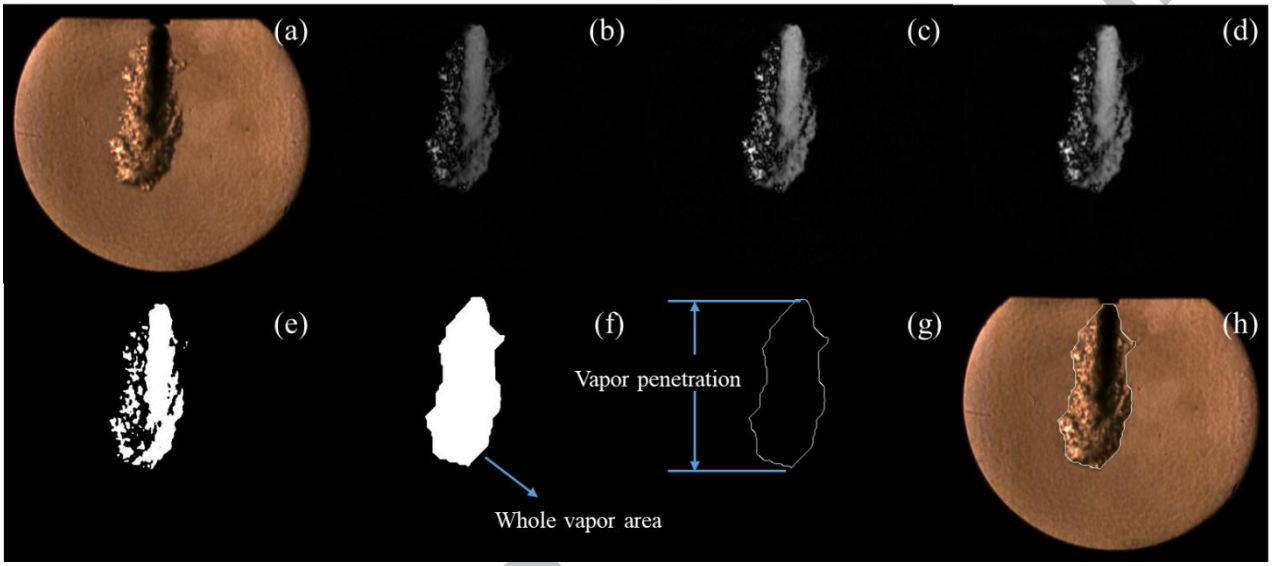

Figure 4. Image processing of Schlieren picture and the definitions of vapor penetration and whole vapor area

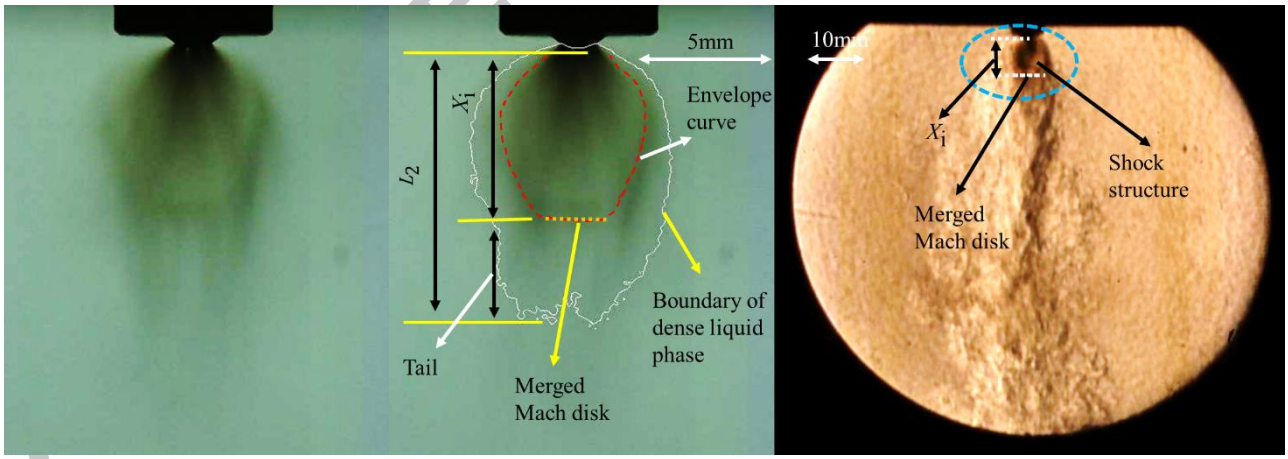

(a) (b) (c)

Figure 5. Measurement of Mach disk distance X_i

3. Result and discussion

3.1 Comparison of trans-critical spray and flash boiling spray

Figure 6 illustrates the spray images by backlit and Schlieren imaging method under different fuel temperatures, and the images were captured at 750 μs after the start of injection (ASOI). The injection pressure was 120 bar, and the ambient

pressure and temperature are fixed at 1 bar and 20 °C, respectively. The spray pattern transits from a flash boiling spray to a trans-critical spray as the fuel temperature increases. The liquid phase has a curve profile near the injector tip for all the spray conditions, and the far end becomes awl-shaped as the fuel temperature increases because high temperature speeds up the evaporation rate. The morphology of those sprays shows the existence of collapse of jet plumes. The mechanism of the collapse could be explained by the theory in Ref. [33]. The fierce interaction between the plumes limit the transfer of the ambient gas from the outside to the closed central region, leading to pressure drop as the spray develops, and the pressure differential between the central region and ambient gas results in the collapse of the plumes. Another theory in Ref. [34] may also explain the mechanism of the collapse. Both the theories concluded that the collapse was attributed to the decrease in pressure in the central region.

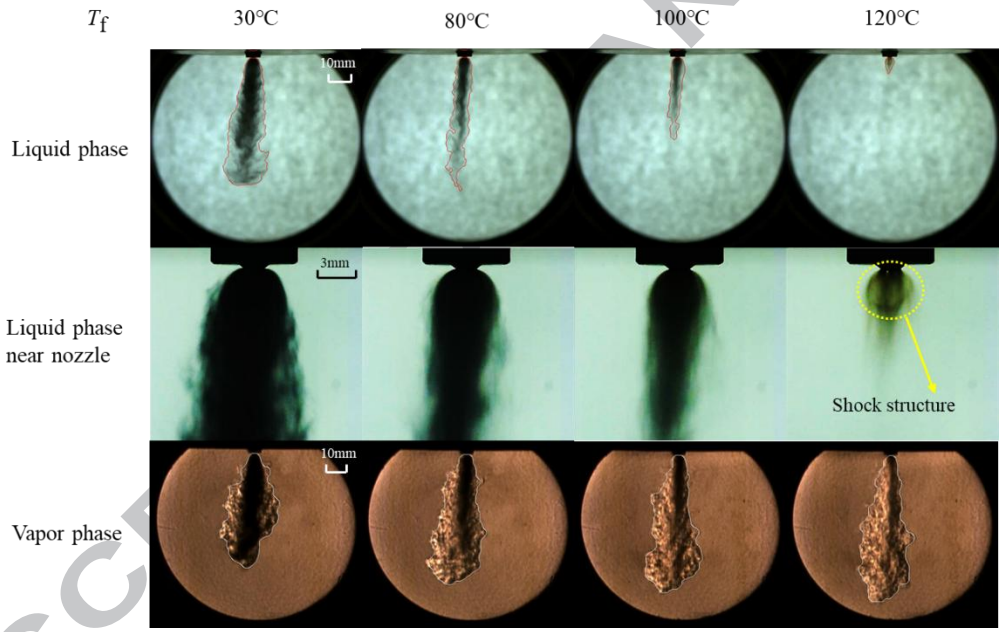

Figure 6. Liquid phase and vapor phase of flash-boiling spray and trans-critical spray of propane at 750 μs ASOI (under p_f=120 bar p_a=1 bar, T_a=20 °C)

The vapor penetrations and the whole vapor areas under different fuel temperatures are shown in Figure 7(a) and Figure 7(b), respectively. As the temperature increases from 30 °C to 120 °C, the vapor penetration moderately increases by 20% and the whole vapor area increases by 14.5% at 1000 μs ASOI. In fact, the supercritical fluid transforms into gas or liquid phase rapidly inside the nozzle and near the nozzle tip due to the rapid local pressure drop and heat transfer. As a result, most of the vapor phase in the spray region is in a normal or superheated state. Therefore, the difference in the vapor

phase area between the flash boiling and trans-critical spray is not significant. Higher fuel temperature can induce stronger interaction among spray plumes, which happens to both types of spray and makes the merged plume thinner and sharper; eventually reducing the head-on resistance [35]; in addition, the high fuel temperature reduces the fuel viscosity, which reduces the drag force and increases the diffusion rate. All these factors contribute to the increase of the vapor penetration and whole vapor area.

Figure 7(c) shows the development of liquid penetration. The liquid penetration at $\bar{T}_r$=0.96 is larger than that at $\bar{T}_r$=0.82 in the early stage, due to less resistance to the thinner spray plume caused by stronger merging. However, the penetration of $\bar{T}_r$=0.96 reaches its maximum earlier than that of $\bar{T}_r$=0.82, due to a higher evaporation rate. The error bar of $\bar{T}_r$=0.96 becomes larger when it reaches its maximum, the boundary is fuzzy, and the uncertainty derived from the imaging process becomes larger. When the fuel temperature increases to $\bar{T}_r$=1.01, the spray changes into trans-critical spray, and the maximum liquid penetration is significantly shorter than that of $\bar{T}_r$=0.96. The liquid penetration dramatically decreases by about 80% when $\bar{T}_r$ changes from 1.01 to 1.06 at 1000 μs ASOI. Overall, the liquid penetration decreases by about 87% from 30 °C to 120 °C. When the liquid penetration reaches the maximum length at about 350 μs ASOI for $\bar{T}_r$=1.01, the curve fluctuates because of the fluctuation of the spray tip, which reflects the turbulent motion of the sprays. In addition, the error bar increases because the boundary of the spray tip becomes indistinct, and the error from image process increases as the fuel temperature increases. At $\bar{T}_r$=1.06, the shock structures quickly establish after the injection, and the tail region is also small because of rapid evaporation under high temperature. Thus, the liquid penetration At $\bar{T}_r$=1.06 is very short, and the liquid boundary is relatively stable, making the amplitude of fluctuation of liquid penetration rather small. In Figure 7(d), the development of the dense liquid phase area generally has the same tendency as the data shown in Figure 7(c). This area decreases by about 97% from 30 °C to 120 °C at 1000 μs ASOI.

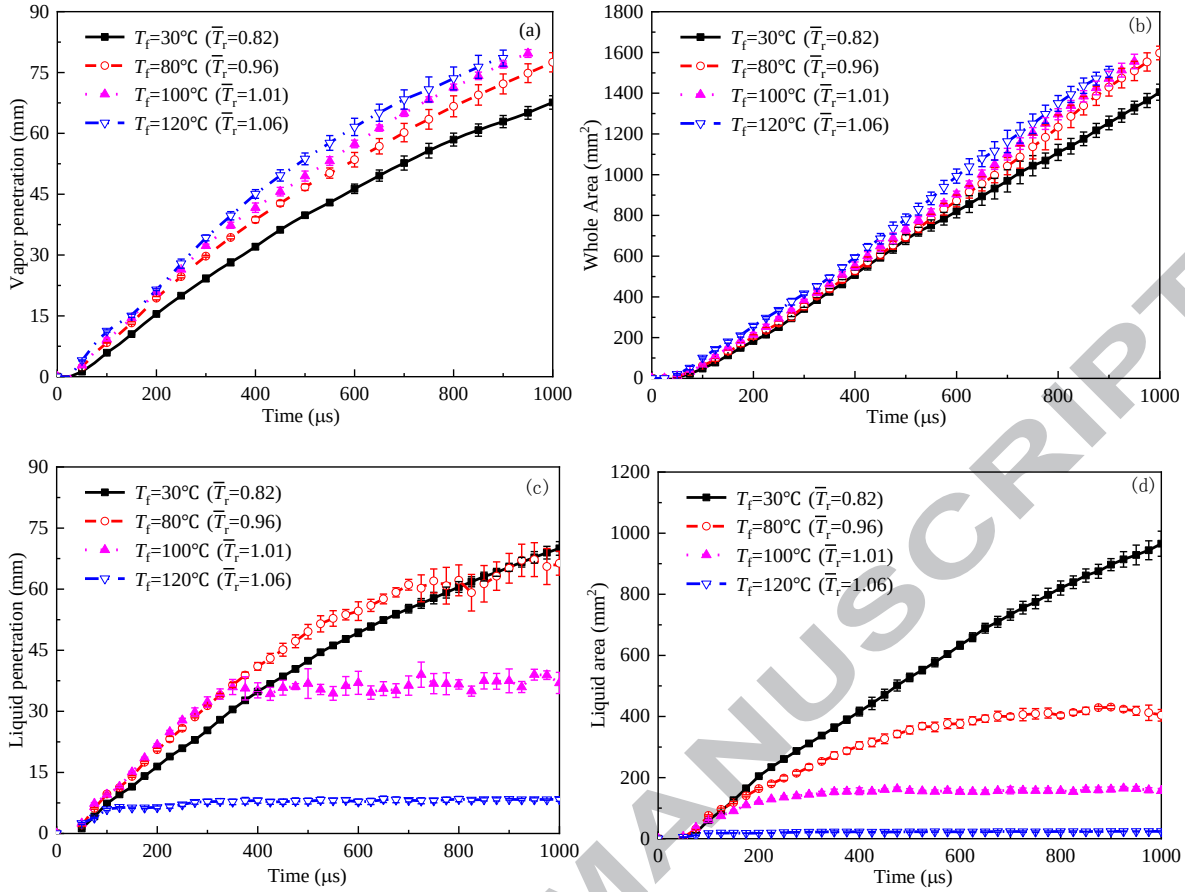

Figure 7. (a) vapor penetration, (b) whole vapor area, (c) liquid penetration, (d) area of dense liquid phase under different fuel temperatures (p_f=120 bar, p_a=1 bar, T_a=20 ℃)

Figure 8 provides a comparison of sprays at T_f=30 ℃ and trans-critical sprays (T_f=120 ℃) under different ambient pressures at 750 μs ASOI. At T_f=30 ℃, the spray under almost ambient pressures (p_a≤5 bar) belong to flash boiling sprays, and the penetration of the spray keeps reducing as the ambient pressure increases. The sprays at this fuel temperature collapse towards the injector spray center at low and high ambient pressures. The mechanism of the spray collapse under different ambient pressures could be found in Ref. [34] [36]. For the trans-critical spray (T_f=120 ℃), the collapse of the spray plumes is fierce at lower ambient pressure, and the individual spray plumes can be distinguished at an elevated pressure. The size of the shock structures decreases as the ambient pressure increases. An interesting tendency is that the length of the trans-critical spray is longer at high ambient pressures. Furthermore, there is no evident entrainment observed in trans-critical spray, and the spray plumes of the trans-critical spray are much thinner than those at T_f =30 ℃ under elevated ambient pressure. The reason for this phenomenon in the trans-critical sprays will be discussed in a later section. The Schlieren images in the same experimental conditions are shown in A2 in the Appendix. For the two fuel temperatures,

the vapor penetration decreases as the ambient pressure increases.

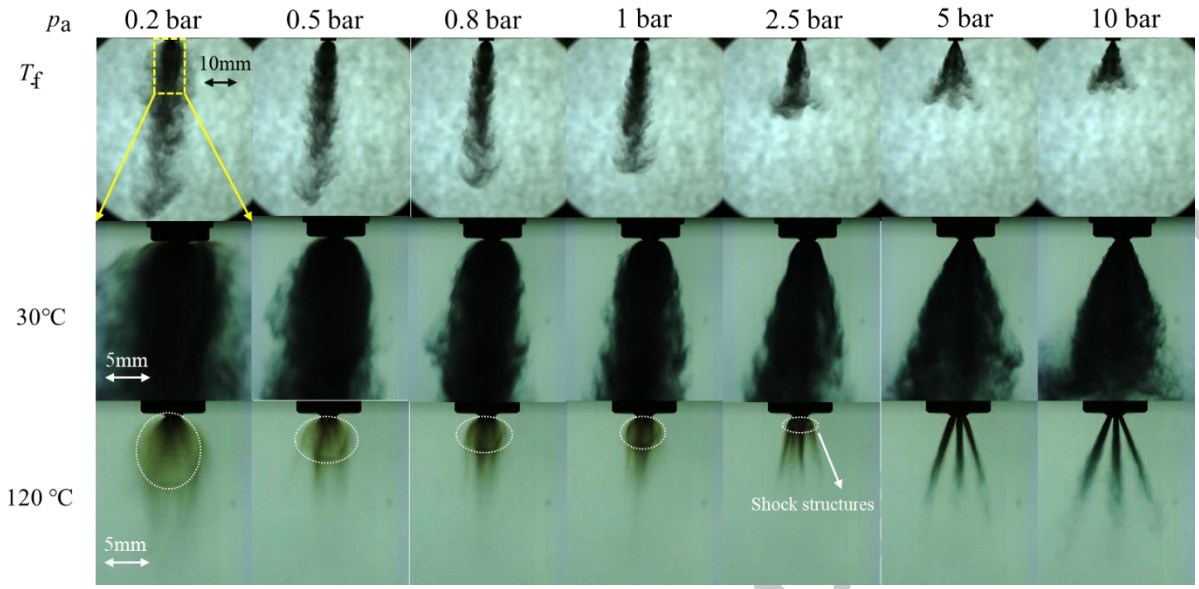

Figure 8. Sprays under different ambient pressures at 750 μs ASOI (under p_f=120 bar, T_a=20 °C)

3.2 The effect of fuel condition on trans-critical spray

3.2.1 Morphology of trans-critical spray

Figure 9 shows the vapor phase and dense liquid phase of the trans-critical sprays under two fuel temperatures (100 °C, 120 °C) and three injection pressures (60 bar, 90 bar, 120 bar). The images of the sprays near the nozzle tip are also presented after careful treatment to show the shape and structure of the sprays near the injector tip. When the fuel temperature is at 100 °C, the interaction among the plumes seems less intense at an injection pressure of 60 bar due to less injection mass and a lower extent of expansion, and the interaction becomes fiercer as the injection pressure increases. Some translucent shock structures can be distinguished at 60 bar injection pressure; it is assumed that those shock structures must exist under higher injection pressure because of higher expansion. However, they disappear. It is attributed to the masking effect of the liquid droplets.

When the fuel temperature increases to 120 °C, the shock structures at the exits of the orifices can be observed at 120 bar injection pressure, the appearance of shock structures is a typical feature of highly under-expanded jets. As the injection pressure decreases, the spray becomes more transparent, namely the proportion of the liquid phase decreases. The disappearance of the dense liquid phase under the fuel condition of 120 °C and 60 bar indicates the existence of a complete gas spray. This phenomenon will be discussed via the analysis of thermodynamic path of injection. According to previous

studies [19][37][22][23][38], the dense liquid phase in the trans-critical spray is condensation-induced liquid due to the sharp decrease in temperature during the dramatic expansion, and the source of the liquid phase in this paper will be discussed later.

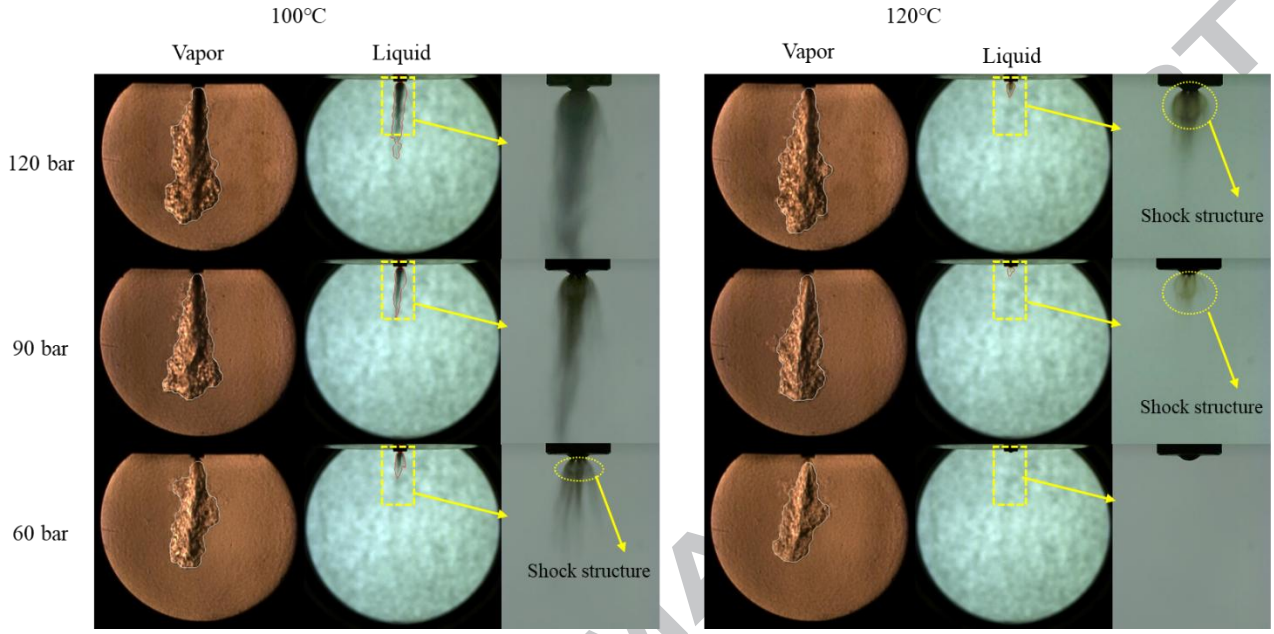

Figure 9. Vapor and liquid phase of trans-critical spray (T_f=100 °C, 120°C) captured 750 μs ASOI (under p_a=1 bar, T_a=20 °C)

3.2.2 Analysis of thermodynamic path

In Figure 10, the pressure-enthalpy diagram of propane, drawn by the software REFPROP [39], is used to analyze the thermodynamic paths of the trans-critical sprays during injection. In this diagram, the black dots represent the initial thermodynamic states of propane, and the ambient pressure is 1 bar. The orange dashed lines are spinodal curves, and the area between the two spinodal curves is an unstable region where the gas phase and liquid coexist. The metastable region between the saturated liquid curve and the liquid spinodal curve is a superheated liquid region and the area on the gas phase side is a supersaturated vapor region [40]. The spinodal curves were firstly acquired by using MBWR (modified Benedict-Webb-Rubin) equation with the criterion $\mathrm{d}p/\mathrm{d}V=0$ in the *p*-*V* diagram, and then drawn in the *p*-*s* diagram. The corresponding *p*-*V* and *T*-*s* diagram are shown in A3 and A4 of the Appendix, respectively. Wu et al. [19] proposed that the expansion could be regarded as an isentropic process, symbolized by the blue dashed arrow line. In fact, if the pressure at the nozzle exit is higher than the ambient pressure, it will lead to a non-isentropic expansion outside the nozzle. Moreover,

the heat transfer and phase transition inside the nozzle lead to entropy increase in the real injection process. The red dashed-dotted arrow lines can indicate the actual thermodynamic paths. It should be noticed that the thermodynamic path shown in Figure 10 refers to the rapid depressurization process inside the injector holes and shock structures. The pressure of the fuel is equal to the ambient pressure near the nozzle exit (no choking conditions) and the boundary of shock structures (choking conditions). The air-fuel mixing process has little effect on the thermodynamic path.

According to the method mentioned in Refs. [19][41], for trans-critical spray, the pressure and the velocity at the nozzle exit can be calculated by the enthalpy conservation equation to determine whether the flow is choked or not. In the beginning, the specific entropy s_f and the enthalpy h_f for the injection are calculated. The physical properties alone the isentrope line can be calculated by REFPROP[39] at different pressures. After that, a first estimate of the nozzle exit pressure $p_{f,e} > p_a$ is made and the fluid enthalpy $h_{f,e}$ and the speed of sound $a_{f,e}$ are derived. The thermodynamic state of the fuel at the nozzle exit is then determined by the enthalpy conservation equation for the estimated exit pressure and the initial injection entropy. Comparison of $u_{f,e}$ with the estimated speed of sound $a_{f,e}$ defines the next step. For subsonic outflow $Ma_{f,e}<1$, the estimated nozzle exit pressure $p_{f,e}$ is successively lowered until either of the following termination conditions is achieved:1.) $Ma_{f,e}=1$ and $p_{f,e}>p_a$, resulting in a choked nozzle flow and sonic velocity at the nozzle exit or 2.) $Ma_{f,e}<1$ and $p_{f,e}=p_a$, resulting in a subsonic jet. In the opposite situation, namely supersonic outflow $Ma_{f,e}>1$, $p_{f,e}$ is successively increased until one of the before mention termination conditions is achieved[41].

The flows are choked for those three different injection pressures at $\bar{T}_r=1.06$ and they result in shock structures that can be clearly distinguished in Figure 9. The thermodynamic states at nozzle exit under three choking conditions are represented by blue squares in Figure 10 and are listed in Table 2. Since the flow is choked, the exit speed is sonic, and the pressure at the nozzle exit is higher than the ambient pressure, leading to the generation of shock structures. However, it is hard to calculate the exit pressure for $\bar{T}_r=1.01$ because the propane will enter into a two-phase region according to this kind of method, and there are no reliable data available to calculate the local pressure and local sonic speed at the nozzle exit. Nevertheless, those shock structures exist in this condition according to Figure 9. The method to determine whether a choking happens in Ref. [41] is not suitable for those conditions under which the supercritical fluid quickly changes into a

liquid phase and enters the two-phase zone. As shown in Table 2, the fluid is in a gas state at the exit of the nozzle when the injection pressure is at 60 bar, makes a pure gas jet possible.

Based on Ref. [42], the liquid phase, namely the opaque area in the backlit images is generated via two different ways. One way is that the transition path could gradually cross the saturated liquid line and superheated liquid region, and eventually enter into the unstable region, as marked by the blue dashed arrow line *AB*, where flash boiling spray occurs. In this case, the cavities generate in the continuous liquid and explode to promote the breakup of the spray [43]. The other path, like the isentropic process of the trans-critical spray, from point C to point D, crosses the vapor saturation curve and vapor spinodal curve. During this process, the trans-critical fuel first changes into vapor and then the supersaturated vapor condenses into the liquid droplets. At the condition $\bar{T}_r$=1.06, $\bar{p}_r$=1.41, the dense liquid phase cannot be observed. The transition line EF does not cross the vapor spinodal line and just enter the vapor metastable zone. For the real transition EF', it departs even further from the vapor spinodal. Perhaps the path does not even enter into the two-phase zone. Therefore, the fuel remains in the gas phase and the condensation hardly occurs during the injection. Thus, the spray is similar to the jet of the ideal gas.

At the same fuel temperature ($\bar{T}_r$=1.06), when the injection pressure increases to $\bar{p}_r$=2.11 (p_f=120 bar), the fluid at the nozzle exit is close to the supercritical state. The thermodynamic path crosses the liquid spinodal curve and extends to the two-phase region. The liquid phase mainly comes directly from supercritical fluid instead of superheated critical. Unlike general flash boiling spray, gas bubbles are generated rapidly outside the nozzle because of the choking phenomenon. The transition path for $\bar{p}_r$=2.82 shows the same trend, but its proportion of liquid phase is larger than that of $\bar{p}_r$=2.11. The liquid droplets in the 'tail region' of the trans-critical sprays under those two injection pressures mainly originate from the transition of a supercritical fluid instead of the condensation of a supersaturated gas.

According to the end position of the thermodynamic path, the proportion of liquid phase in the 'tail region' increase with the ambient pressure. The spray at $\bar{T}_r$=1.01 and $\bar{p}_r$=2.82 can also be classified as a trans-critical spray. However, it is very similar to the flash boiling spray of propane because its transition path is similar to the flash boiling spray (T_f=30 °C); on the other hand, the shock structures also exist in this condition according to the previous discussion. The choking

phenomenon and shock structures can exist under near-critical fuel condition, the masking effect of droplets should be taken into consideration when finding the shock structures. The similar profiles of the sprays near the nozzle indicate that, under certain operating conditions, flash boiling sprays also present choking phenomenon and shock structures, which cannot be observed because of masking effect.

In this paper, all the flash-boiling sprays have a similar injection process whatever the fuel condition is because they have the same transition path. In contrast, the fuel condition has a significant effect on the spray pattern of the trans-critical spray because the initial fuel state determines which areas of the *p-s* diagram the thermodynamic paths will cross. As for a trans-critical spray, a lower injection pressure makes it easier for the expansion path to enter the gas zone; when the injection pressure decreases to a certain value, the liquid phase disappears, and the trans-critical spray becomes a gas-like jet; a higher fuel temperature also makes the gas-like jet more possible.

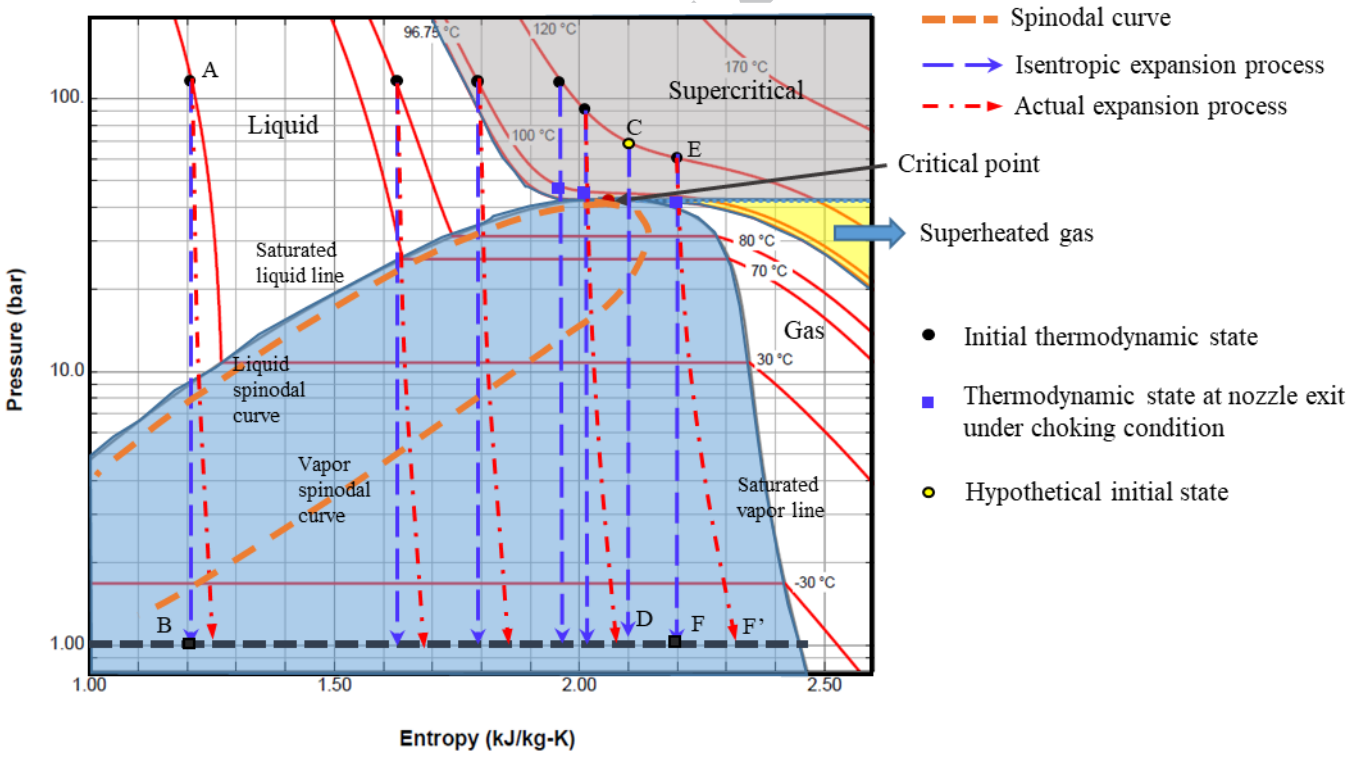

Figure 10. Propane pressure-enthalpy diagram and thermodynamic paths for different thermal conditions

Table 2 Nozzle exit properties for choking conditions

Fuel temperature (°C)	Injection pressure (bar)	Nozzle exit pressure (bar)	Nozzle exit temperature (°C)	Sonic velocity (m/s)	Thermodynamic state

120	120	47.9	99.88	204.6	Supercritical
120	90	47.2	101.36	166.5	Supercritical
120	60	40.2	94.12	151.6	Gas phase

3.2.3 Mach disk distance in trans-critical spray

Two dimensionless numbers, non-dimensional Mach disk distance X_i/D and pressure ratio p_f/p_a, are introduced here. X_i is the length of the Mach disk distance and D is the diameter of a single hole of the injector. The calculated values for the trans-critical spray (T_f=120 °C) under different injection pressures and ambient pressures are presented in Figure 11 (represented by black squares). A blue line with round dots is drawn by the formula suitable for the overexpansion of the under-expanded ideal gas [44]. It is obtained from a single-nozzle injection, providing an equation form [44][45][46][47]:

$$X_i/D = C_x \left(\frac{p_f}{p_a}\right)^{0.5} \quad (1)$$

C_x can vary from fuel to fuel [47], but is close to 0.5.

In theory, the trans-critical spray has the same tendency as the expansion of the under-expanded ideal gas. However, the Mach disk distance of this experiment diverges from the ideal gas jet, due to the interaction among those five Mach disk-shaped plumes. Eq. (1) needs modification for a better fitting, so another parameter should be added. According to the experimental result, there must be a threshold of p_f/p_a to generate choking flow and shock structures because the shock structures disappear at elevated ambient pressure and the function can be assumed as:

$$X_i/D = C_x \left(\frac{p_f}{p_a} - \alpha\right)^{0.5} \quad (2)$$

α is related to the threshold of choking. Through using the least square fitting method, the derived C_x gives a value of 1.54 and α is 31.5. The R^2 of this fitting equation is 0.99. C_x in the present study is much larger than that of the under-expanded gas jet, and this may be due to the fierce interaction of those five shock structures, which could be lengthened. The effects of interaction among sprays need to be considered in detail in further research. For the cases at an injection pressure of 120 bar, the values of p_f/p_a at ambient pressure of 5 bar and 10 bar are 24 and 12 respectively, which are under the threshold of 31.5. In these cases, the values gained from Eq. (2) are negative numbers, indicating the shock structures disappear or its size can be negligible under the corresponding conditions (shown in Figure 8).

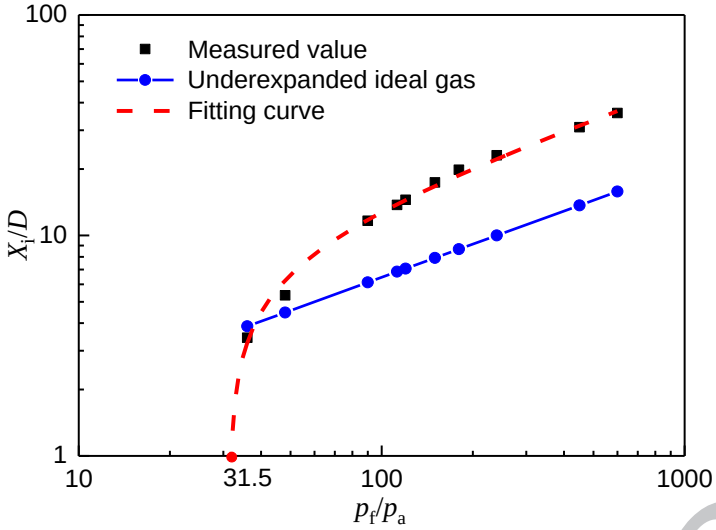

Figure 11. Non-dimensional Mach disk distance X_i/D versus pressure ratio (under T_f=120 °C, T_a=20 °C)

3.3 Effect of ambient pressure on the liquid length

As shown in Figure 12(a), the ambient pressure has complicated effects on the penetration of the dense liquid phase of the trans-critical spray. The penetration of the dense liquid phase decreases with the ambient pressure increasing at the first stage of injection. However, the curves also fluctuate after reaching their maximums. The average maximum values, namely the liquid length, between 400 μs and 1000 μs are calculated for comparison, as shown in Figure 12(b). The liquid length varies non-monotonously with the increase in ambient pressure. However, as shown in Figure 12(c), the vapor decreases continuously as the ambient pressure increases. It is no doubt that the expansion and evaporation dominate the vapor penetration. As the ambient pressure rises, the resistance for expansion and evaporation increases, meanwhile, the speed of the spray decreases more rapidly.

At p_a=0.2 bar, the expansion of the spray is the most intense and the shock structures are enormous in comparison with the hole's diameter. This leads to a fierce plume interaction and plume merging, and eventually, it results in a long liquid length even though the evaporation rate is relatively high. Under low ambient pressures (p_a≤0.5 bar), increasing back pressure reduces the expansion of the spray [48][49] and decreases the size of shock structures and Mach disk distance X_i, (shown in Figure 8). This same tendency was also observed in the cases of the under-expanded ideal gas [50]. Those factors dominate the process of spray and shorten the maximum penetration.

From p_a=0.5 bar to p_a=1 bar, the liquid length remains almost the same. A high ambient pressure diminishes the size of shock structures. However, the proportion of liquid phase increases and the evaporation slows down. The competition of

those effects generally produces a balance. Thus the maximum penetration only slightly varies. The maximum liquid penetration reaches its lowest value when the ambient pressure increases to 2.5 bar. Elevated ambient pressure prohibits the spray expansion and causes a sharp drop in the size of the shock structures. The increased drag force also reduces the penetrations. Those effects contribute to the decrease in the maximum penetration of dense liquid phase.

However, at an ambient pressure higher than 2.5 bar, the shock structures are negligible, the slow evaporation and the high proportion of liquid phase finally dominate the spray development and the dense liquid phase tends to increase as the ambient pressure increases. Under elevated ambient pressures, the formation of vapor phase from the supersaturated liquid also happens according to Figure 10. The gas bubbles generate and grow up in the interior of the plume and promote the breakup of the liquid media. However, the evaporation rate is relatively high compared to the generation of liquid droplets, eventually forming a thin liquid plume. As the ambient pressure increases, the generation rate of the gas bubbles, evaporation rate and expansion of plumes decrease, the interaction between the plumes becomes weaker. The pressure in the central region of the spray and ambient pressure can rapidly achieve a balance, and the collapse disappears. The individual thin plume, therefore, can be distinguished (shown in Figure 8).

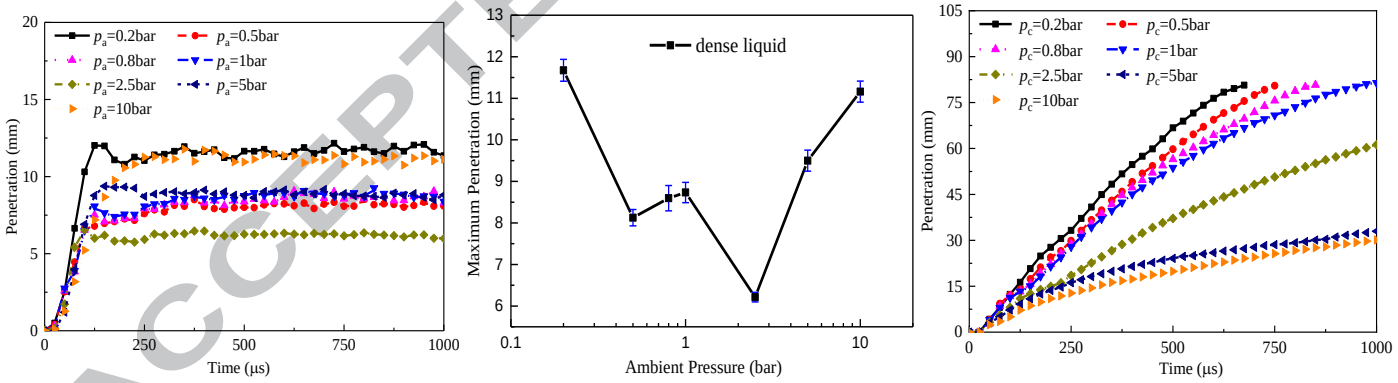

(a) (b) (c)

Figure 12. (a) Variation of liquid penetration with time, (b) liquid length under different ambient pressures, (c) Variation of vapor penetration with time (p_f=120 bar, T_f=120 °C, T_a=20 °C)

4. Conclusion

Macroscopic properties of the trans-critical spray of propane have been investigated using high-speed Schlieren and backlit imaging methods. The effects of injection pressure, ambient pressure and fuel temperature on the macroscopic

characteristics of spray, including the penetration length, spray area, and Mach disk distance, were analyzed. The thermodynamic path was discussed via a *p*-*s* diagram to reveal the unique phenomenon of trans-critical spray. The main conclusions are summarized as follows:

1) The multi-hole trans-critical spray has clear shock structures at fuel temperature beyond T_f=120 °C when the injection pressure is high enough. Due to the interaction among plumes, the shock structures are distorted by the collapse effect. The liquid phase disappears when the injection pressure decreases to 60 bar because the path departs from the vapor spinodal line, perhaps the path does not even enter into the two-phase zone. The trans-critical fluid first changes to the super-heated gas and then cools down as in a gas state. To obtain a gas-like jet, the fuel temperature should be high enough, and the injection pressure should be limited.
2) Shock structures may exist at fuel temperature of 100 °C, masking effect should be taken into consideration. A flash-boiling spray may present choking phenomenon and shock structures, however, the masking effect of droplets weakens their imaging process.
3) The Mach disk distance of the current multi-hole trans-critical spray under T_f=120 °C is larger than that derived from the jet of under-expanded ideal gas. This difference can be attributed to the interaction of spray plumes; X_i/D has a close correlation with p_f/p_a, it gives an exponential form. There is a threshold below which the shock structures disappear.
4) As ambient pressure increases, the liquid length initially decreases when the ambient pressure varies from 0.2 bar to 0.5 bar, then it stays at the same until 1 bar, and it decreases to its minimum at 2.5 bar. When ambient pressure continues to increase, the liquid length starts to increase.

In future research, the characteristics such as Sauter mean diameter (SMD) and local velocity will be investigated to give an in-depth insight of the trans-critical spray of propane. The similarity of the expansion process between flash boiling and trans-critical sprays under normal or low ambient pressure will also be further studied.

Acknowledgments

This research was sponsored by the National Natural Science Foundation of China under Grant 51506111.

Reference

[1] Wang JM, Jeong CH, Zimmerman N, Healy RM, Wang DK, Ke F, et al. Plume-based analysis of vehicle fleet air pollutant emissions and the contribution from high emitters. Atmospheric Measurement Techniques 2015;8:3263–75. doi:10.5194/amt-8-3263-2015.

[2] Lepert P, Brillet F. The overall effects of road works on global warming gas emissions. Transportation Research Part D: Transport and Environment 2009;14:576–84. doi:10.1016/j.trd.2009.08.002.

[3] Lawankar SM. Influence of Compression Ratio and Ignition Timing on the Performance of LPG Fuelled SI Engine. SAE Technical Paper 2013-01-2889; 2013. doi:10.4271/2013-01-2889.

[4] Mizushima N, Sato S, Ogawa Y, Yamamoto T, Sawut U, Takigawa B, et al. Combustion Characteristics and Performance Increaseof an LPG-SI Engine with Liquid Fuel Injection System. SAE Technical Paper 2009-01-2785; 2009. doi:10.4271/2009-01-2785.

[5] Morganti K, Foong TM, Brear M, Da Silva G, Yang Y, Dryer F. Design and Analysis of a Modified CFR Engine for the Octane Rating of Liquefied Petroleum Gases (LPG). SAE International Journal of Fuels and Lubricants 2014;7:283–300. doi:10.4271/2014-01-1474.

[6] Morganti KJ, Foong TM, Brear MJ, da Silva G, Yang Y, Dryer FL. The Research and Motor octane numbers of Liquefied Petroleum Gas (LPG). Fuel 2013;108:797–811. doi:10.1016/j.fuel.2013.01.072.

[7] Bonatesta F, Chiappetta E, La Rocca A. Part-load particulate matter from a GDI engine and the connection with combustion characteristics. Applied Energy 2014;124. doi:10.1016/j.apenergy.2014.03.030.

[8] Storey J, Barone T, Thomas J, Huff S. Exhaust Particle Characterization for Lean and Stoichiometric DI Vehicles Operating on Ethanol-Gasoline Blends. SAE Technical Paper 2012-01-0437; 2012. doi:10.4271/2012-01-0437.

[9] Jang J, Lee J, Kim J, Park S. Comparisons of the nanoparticle emission characteristics between GDI and PFI vehicles. Journal of Nanoparticle Research 2015;17:1–14. doi:10.1007/s11051-015-3280-2.

[10] Yinhui W, Rong Z, Yanhong Q, Jianfei P, Mengren L, Jianrong L, et al. The impact of fuel compositions on the particulate emissions of direct injection gasoline engine. Fuel 2016;166:543–52. doi:10.1016/j.fuel.2015.11.019.

[11] Gitano-briggs H, Faizi MUSTAFA K, Yew Heng T, Chang Yew S. LPG Direct Injection: An Alternative Fuel Solution to the Two-Stroke Emissions Problem. SAE Technical Paper 2007-32-0024; 2007.

[12] Kim K, Kim J, Oh S, Kim C, Lee Y. Evaluation of injection and ignition schemes for the ultra-lean combustion direct-injection LPG engine to control particulate emissions. Applied Energy 2017;194:123–35. doi:10.1016/j.apenergy.2017.03.012.

[13] Kim K, Kim J, Oh S, Kim C, Lee Y. Lower particulate matter emissions with a stoichiometric LPG direct injection engine. Fuel 2017;187:197–210. doi:10.1016/j.fuel.2016.09.058.

[14] Myung CL, Choi K, Kim J, Lim Y, Lee J, Park S. Comparative study of regulated and unregulated toxic emissions characteristics from a spark ignition direct injection light-duty vehicle fueled with gasoline and liquid phase LPG (liquefied petroleum gas). Energy 2012;44:189–96. doi:10.1016/j.energy.2012.06.039.

[15] Mesman PH, Veenhuizen B. The Spray Behavior of Liquid LPG at Different Back Pressures During Injection in a Constant Volume Chamber. SAE Technical Paper 2009-01-1834; 2009. doi:10.4271/2009-01-1834.

[16] Lacey JS, Pourzakadeh F, Brear M, Petersen P, Lakey C, Ryan S, et al. Optical Characterization of Propane at Representative Spark Ignition , Gasoline Direct Injection Conditions. SAE Technical Paper 2016-01-0842; 2016. doi:10.4271/2016-01-0842.

[17] Haynes WM. CRC Handbook of Chemistry and Physics, 95th Edition, 2014-2015. vol. 54. 2014. doi:10.1136/oem.53.7.504.

[18] Segal C, Polikhov SA. Subcritical to supercritical mixing. Physics of Fluids 2008;20:052101. doi:10.1063/1.2912055.

[19] Wu P-K, Chen TH, Nejad AS, Carter CD. Injection of supercritical ethylene in nitrogen. Journal of Propulsion and Power 1996;12:770–7. doi:10.2514/3.24100.

[20] Wu P-K, Shahnam M, Kirkendall KA, Carter CD, Nejad AS. Expansion and Mixing Processes of Underexpanded Supercritical Fuel Jets Injected into Superheated Conditions. Journal of Propulsion and Power 1999;15:642–9. doi:10.2514/2.5488.

[21] Star AM, Edwards JR, Lin K-C, Cox-Stouffer S, Jackson TA. Numerical Simulation of Injection of Supercritical Ethylene into Nitrogen. Journal of Propulsion and Power 2006;22:809–19. doi:10.2514/1.16621.

[22] Lin K-C, Cox-Stouffer S, Kennedy PJ, Jackson TA. Expansion of Supercritical Methane/Ethylene Jets in a Quiescent Subcritical Environment. 41st Aerospace Sciences Meeting and Exhibit 2003. doi:10.2514/6.2003-483.

[23] Lin K, Jackson TA. Structures and Phase Transition Processes of Supercritical Methane / Ethylene Mixtures Injected Into a Subcritical Environment Phase Transition Processes of Supercritical Methane / Ethylene Mixtures Injected. Combustion Science and Technology 2007;178:129–60. doi:10.1080/00102200500290716.

[24] De Boer C, Bonar G, Sasaki S, Shetty S. Application of Supercritical Gasoline Injection to a Direct Injection Spark Ignition Engine for Particulate Reduction. SAE Technical Paper 2013-01-0257; 2013. doi:10.4271/2013-01-0257.

[25] Zhang M, Pei Y, Liu Y, Zhang Y. Study on Subcritical / Supercritical Spray Characteristics of a Multi-Hole Gasoline Direct Injector. SAE Technical Paper 2016-01-0849; 2016. doi:10.4271/2016-01-0849.

[26] Li Y, Guo H, Fei S, Ma X, Zhang Z, Chen L, et al. An exploration on collapse mechanism of multi-jet flash-boiling sprays. Applied Thermal Engineering 2018;134:20–8. doi:10.1016/j.applthermaleng.2018.01.102.

[27] Li Y, Guo H, Ma X, Qi Y, Wang Z, Xu H, et al. Morphology analysis on multi-jet flash-boiling sprays under wide ambient pressures. Fuel 2018;211:38–47. doi:10.1016/j.fuel.2017.08.082.

[28] Bar-Kohany T, Levy M. STATE OF THE ART REVIEW OF FLASH-BOILING ATOMIZATION. Atomization and Sprays 2016;26:1259–305. doi:10.1615/AtomizSpr.2016015626.

[29] Hutcherson MN, Henry RE, Wollersheim DE. Two-phase vessel blowdown of an initially saturated liquid—Part 1: Experimental. Journal of Heat Transfer 1983;105:687–93.

[30] Hutcherson MN, Henry RE, Wollersheim DE. Two-phase vessel blowdown of an initially saturated liquid—Part 2: Analytical. Journal of Heat Transfer 1983;105:694–9.

[31] Otsu N. A Threshold Selection Method from Gray-Level Histograms. IEEE Transactions on Systems, Man, and Cybernetics 1979;9:62–6. doi:10.1109/TSMC.1979.4310076.

[32] Sobel I. History and definition of the sobel operator. Retrieved from the World Wide Web 2014.

[33] Wu S, Xu M, Hung DLS, Li T, Pan H. Near-nozzle spray and spray collapse characteristics of spark-ignition direct-injection fuel injectors under sub-cooled and superheated conditions. Fuel 2016;183:322–34. doi:10.1016/j.fuel.2016.06.080.

[34] Guo H, Ding H, Li Y, Ma X, Wang Z, Xu H, et al. Comparison of spray collapses at elevated ambient pressure and flash boiling conditions using multi-hole gasoline direct injector. Fuel 2017;199:125–34. doi:10.1016/j.fuel.2017.02.071.

[35] Zeng W, Xu M, Zhang G, Zhang Y, Cleary DJ. Atomization and vaporization for flash-boiling multi-hole sprays with alcohol fuels. Fuel 2012;95:287–97. doi:10.1016/j.fuel.2011.08.048.

[36] Li Y, Guo H, Ma X, Wang J, Xu H. Droplet dynamics of di spray from sub-atmospheric to elevated ambient pressure. Fuel 2016;179:25–35. doi:10.1016/j.fuel.2016.03.047.

[37] Star AM, Edwards JR, Lin K-C, Cox-Stouffer S, Jackson T a. Numerical Simulation of Injection of Supercritical Ethylene into Nitrogen. Journal of Propulsion and Power 2006;22:809–19. doi:10.2514/1.16621.

[38] Qiu L, Reitz RD. Simulation of supercritical fuel injection with condensation. International Journal of Heat and Mass Transfer 2014;79:1070–86. doi:10.1016/j.ijheatmasstransfer.2014.08.081.

[39] Lemmon EW, Huber ML, McLinden MO. NIST Standard Reference Database 23: Reference Fluid Thermodynamic and Transport Properties (REFPROP), Version 9.0. National Institute of Standards and Technology, Standard Reference Data Programm, Gaithersburg 2010.

[40] Jarvis TJ, Donohue MD, Katz JL. Bubble nucleation mechanisms of liquid droplets superheated in other liquids. Journal of Colloid and Interface Science 1975;50:359–68. doi:10.1016/0021-9797(75)90240-4.

[41] Ingo Stotz, Bernhard Weigand, Grazia Lamanna, Ernst Oldenhof. Disintegration Regimes Near the Critical Point. Proceedings of the 18th AIAA/3AF International Space Planes and Hypersonic Systems and Technologies Conference, 2012. doi:10.2514/6.2012-5914.

[42] Star A, Edwards J, Lin K-C, Jackson T. Modeling of Condensation in Injection of Supercritical Fuels. 44th AIAA

Aerospace Sciences Meeting and Exhibit, Reston, Virigina: American Institute of Aeronautics and Astronautics; 2006. doi:10.2514/6.2006-810.

[43] Sher E, Bar-Kohany T, Rashkovan A. Flash-boiling atomization. Progress in Energy and Combustion Science 2008;34:417–39. doi:10.1016/j.pecs.2007.05.001.

[44] Grist S, Sherman PM. Study of the Highly Underexpanded Sonic Jet. AIAA JOURNAl 1966;4:68–77.

[45] EWAN BCR, MOODIE K. Structure and Velocity Measurements in Underexpanded Jets. Combustion Science and Technology 1986;45:275–88. doi:10.1080/00102208608923857.

[46] Velikorodny A, Kudriakov S. Numerical study of the near-field of highly underexpanded turbulent gas jets. International Journal of Hydrogen Energy 2012;37:17390–9. doi:10.1016/j.ijhydene.2012.05.142.

[47] Rogers T, Petersen P, Koopmans L, Lappas P, Boretti A. Structural characteristics of hydrogen and compressed natural gas fuel jets. International Journal of Hydrogen Energy 2015;40:1584–97. doi:10.1016/j.ijhydene.2014.10.140.

[48] Yu J, Vuorinen V, Kaario O, Sarjovaara T, Larmi M. Visualization and analysis of the characteristics of transitional underexpanded jets. International Journal of Heat and Fluid Flow 2013;44:140–54. doi:10.1016/j.ijheatfluidflow.2013.05.015.

[49] Franquet E, Perrier V, Gibout S, Bruel P. Free underexpanded jets in a quiescent medium: A review. Progress in Aerospace Sciences 2015;77:25–53. doi:10.1016/j.paerosci.2015.06.006.

[50] Hamzehloo A, Aleiferis PG. Gas dynamics and flow characteristics of highly turbulent under-expanded hydrogen and methane jets under various nozzle pressure ratios and ambient pressures. International Journal of Hydrogen Energy 2016;41:6544–66. doi:10.1016/j.ijhydene.2016.02.017.

Appendix

A1. Fuel state at different experiment conditions

Temperature (C)	Pressure (bar)	Density (kg/m3)	Volume (m3/kg)	Internal Energy (kJ/kg)	Enthalpy (kJ/kg)	Entropy (J/g*K)	Sound Spd. (m/s)	Phase
30	120	512.89	0.00195	258.56	281.96	1.2077	860.69	liquid
80	120	444.25	0.00225	391.22	418.23	1.6231	608.95	liquid
100	60	349.25	0.00286	483.39	500.57	1.8898	309.43	supercritical
100	90	389.6	0.00257	461.76	484.86	1.8261	435.05	supercritical
100	120	411.3	0.00243	449.4	478.57	1.7893	515.23	supercritical
120	60	210.6	0.00475	595.51	624	2.2111	180.27	supercritical
120	90	337.7	0.00296	530.64	557.29	2.0151	331.53	supercritical
120	120	373.66	0.00268	511.18	543.29	1.9582	428.86	supercritical

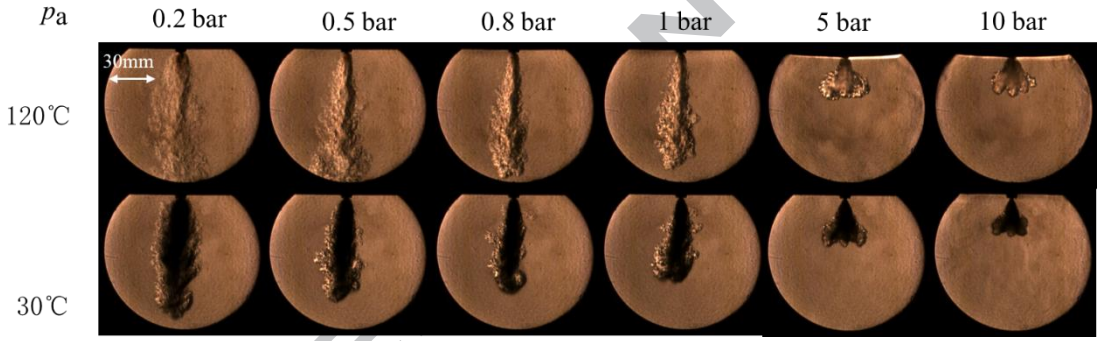

A2. Schlieren images of the sprays under different ambient pressures at 750 μs ASOI (under p_f=120 bar, T_a=20 °C)

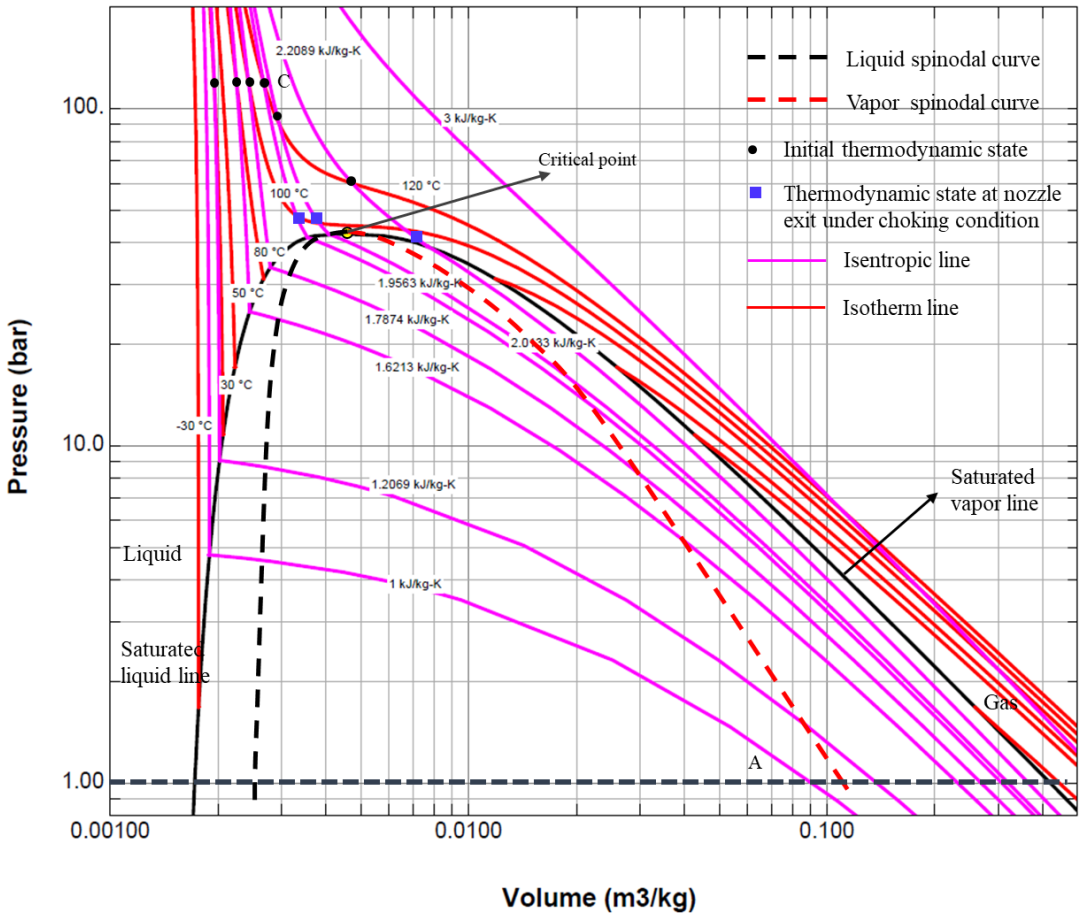

A3. The *p-V* diagram of propane and thermodynamic states for different thermal conditions

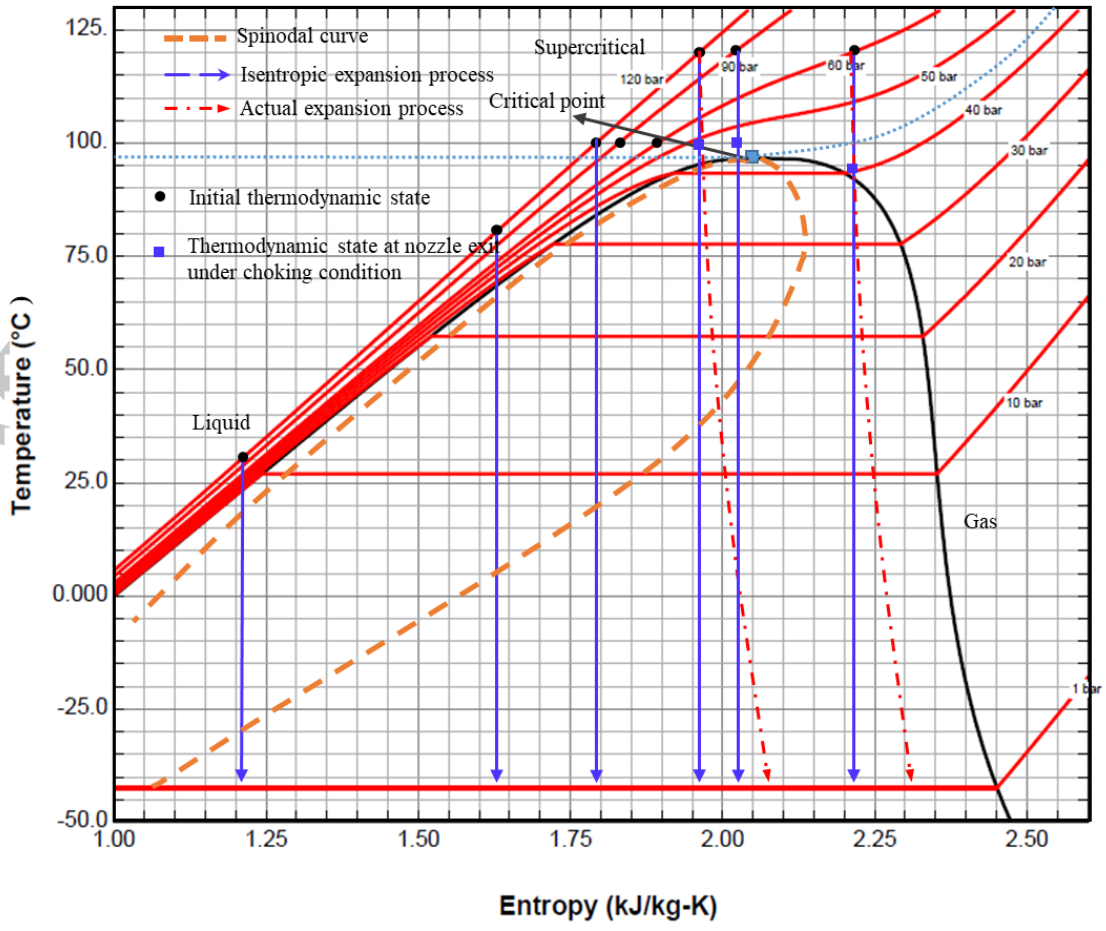

A4. The *T-s* diagram of propane and thermodynamic paths

Highlights

- Trans-critical and flash-boiling sprays of propane show the similarity in spray morphology.
- Shock structures near the nozzle are observed in trans-critical sprays of propane.
- Decreasing the injection pressure of trans-critical spray can induce a gas-like jet.
- Interaction of spray plumes increases Mach disk distance of trans-critical propane spray.